ACS APPLIED ENERGY MATERIALS
Cite This: ACS Appl. Energy Mater. 2019, 2, 8376−8380
Letter
www.acsaem.org

High Photothermally Active Fe_2O_3 Film for CO_2 Photoreduction with H_2O Driven by Solar Light

Zekai Zhang,*[,†] Zhihong Gao,[†] Huayan Liu,[†] Stéphane Abanades,[‡] and Hanfeng Lu*[,†]

[†]Institute of Chemical Reaction Engineering, College of Chemical Engineering, Zhejiang University of Technology, Chaowang Road 18, Hangzhou 310014, China

[‡]Processes, Materials, and Solar Energy Laboratory, PROMES-CNRS (UPR 8521), 7 Rue du Four Solaire, 66120 Font-Romeu, France

Supporting Information

ABSTRACT: A Fe_2O_3 film exhibited high activity for CO_2 photoreduction with H_2O under high solar light intensity and temperature. CH_4, C_2H_4 and C_2H_6 were detected simultaneously, and the maximum generation rates reached 1470.7, 736.2, and 277.2 μmol/(g_{cata}·h), respectively. These results prove the feasibility of the novel approach, and the suitability of iron oxide as a photothermally active catalyst. The noteworthy performance of Fe_2O_3 was arising from the beneficial contribution of the highly photothermal conditions and the formation of a Fe_2O_3/Fe_3O_4 Z-scheme system. The study elucidates the feasibility of photothermal synergistic catalytic effect for solar energy utilization in CO_2 photoreduction.

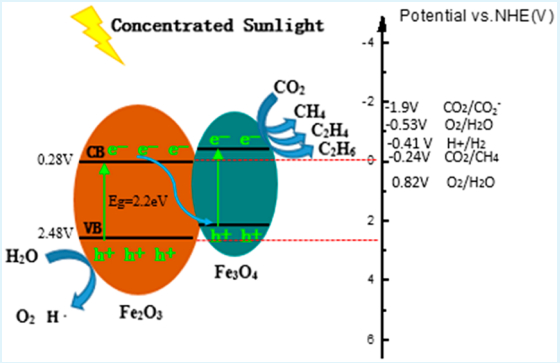

KEYWORDS: *photoreduction, photothermal, Fe_2O_3/Fe_3O_4, CO_2 reduction*

Global CO_2 emissions reached 37 gigatons in 2018, which is twice as much as the amount being absorbed back into nature. Solar energy is the most abundant renewable energy resource, holding the answer to reducing CO_2 emissions from fossil fuels. Combining solar energy with CO_2 and H_2O reduction represents the sunshine to liquid vision to produce green liquid fuels.[1] The use of solar energy to convert CO_2 into hydrocarbons can simultaneously achieve CO_2 emission control, carbon cycle closure, and solar energy storage. In view of reducing the growing CO_2 emissions contributing to global warming, one possible main approach for reaching this objective is photochemical and another is thermochemical CO_2 conversion. The former is known as CO_2 photo(electron-)catalytic reduction or artificial photosynthesis based on the photoelectric effect and represents a promising pathway for CO_2 conversion to fuels and chemical commodities using solar energy.[2,3] The latter is intended to split CO_2 (or H_2O) under extreme high temperatures (often >1000 °C) to produce CO (or H_2) that can be further converted to liquid fuels.[4,5] In addition to the thermochemical route, CO_2 photoreduction is widely developed and under investigation at present. However, due to the wide band gap of semiconductor catalysts, CO_2 photoreduction is usually carried out at room temperature and often only uses short-wavelength light in the solar spectrum (thus it can only convert a small portion of the solar spectrum), while most of the solar energy is converted into low-grade useless heat during the reaction, which restrains the overall solar energy conversion efficiency. Though much attention has been paid to the topic, it still requires strong research efforts to reach a reasonable fuel production range.[6−8]

Recently, the photothermal concept has been developed to effectively use long-wavelength solar light. Some metals are doped into the photocatalyst system to generate the hot charge carriers for CO_2 photoreduction via plasmatic effect.[9,10] Meanwhile, there may exist a more direct and simple way to achieve the same goal. Indeed, the low-grade or low-temperature heat, generated from long-wavelength light, can be raised and upgraded by using concentrated solar light technology. Although CO_2 reduction is a photoelectron catalytic reaction with minor influence of the reaction temperature, it can be expected that such a temperature increase could improve the reaction extent by favoring thermodynamics, even exhibiting a photothermal synergistic catalytic effect.

To achieve this goal, a high thermally active and stable semiconductor catalyst is required, as it is recognized that temperature increase will influence the properties of the semiconductor catalyst, by enhancing the charge recombination in the semiconductor, in turn decreasing the photocatalytic activity. Iron is one of the most common elements in the earth's crust. Iron oxide in the α-phase (α-Fe_2O_3) with a band gap of 2.2 eV has good thermal stability and the

Received: September 17, 2019
Accepted: December 5, 2019
Published: December 5, 2019

DOI: 10.1021/acsaem.9b01825
ACS Appl. Energy Mater. 2019, 2, 8376−8380

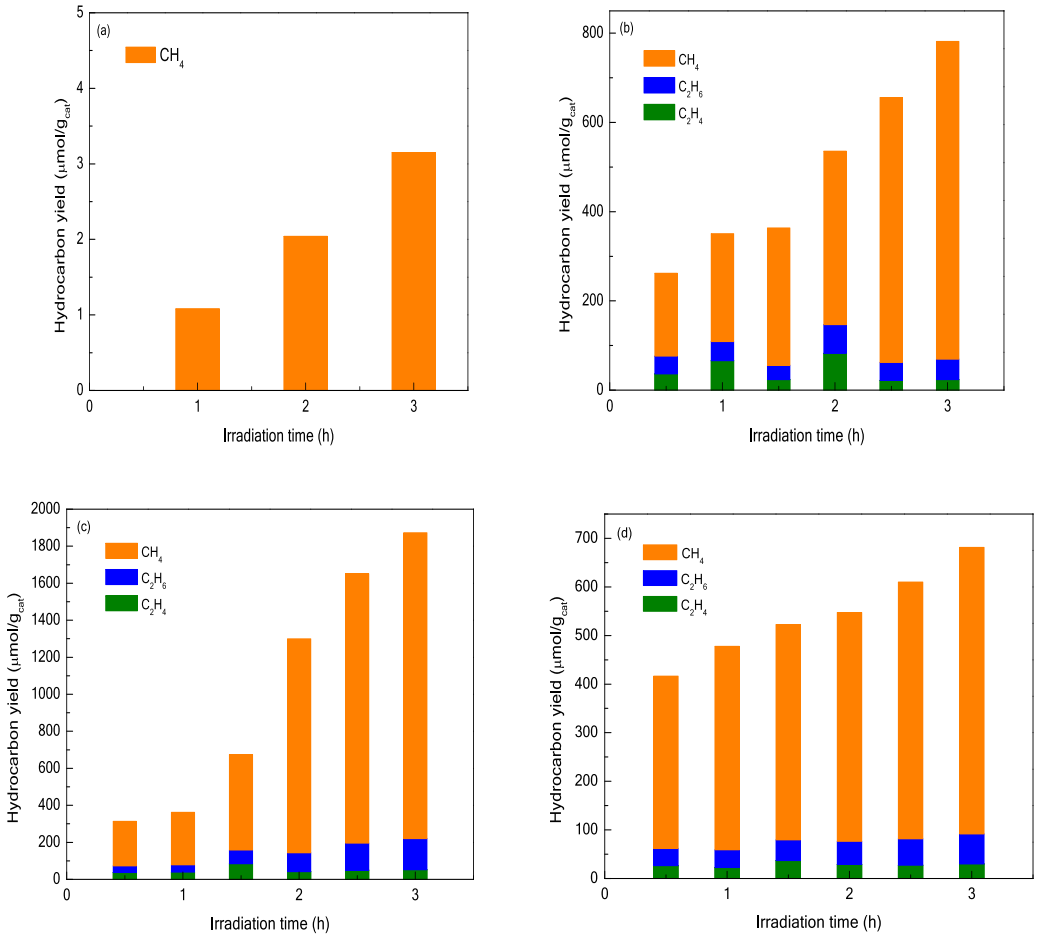

Figure 1. CO_2 photoreduction behavior of Fe_2O_3 film under different concentrating ratios (CRs): (a) natural light (CR = 1), 50 °C; (b) CR = 400, 450 °C; (c) CR = 600, 560 °C; (d) CR = 800, 680 °C.

capability to absorb photons in the visible spectral range; hence, it attracts increasing attention in the CO_2 photoreduction field as a semiconductor photocatalyst.[11,12] Iron oxide can also be found in different oxidation states, being involved in the form of Fe_2O_3/Fe_3O_4 or Fe_3O_4/FeO redox pairs at high temperatures, which is in favor of solar thermochemical splitting of CO_2.[13,14] Therefore, iron oxide is expected to be a suitable candidate catalyst for the CO_2 reduction process. Nevertheless, the low conduction band (CB) bottom level of α-Fe_2O_3 implies photogenerated electrons with low energy, which is unfavorable for carrying out reduction reactions with CO_2 and H_2O. Thus, single α-Fe_2O_3 cannot meet the demand of CO_2 photoreduction. Thus, it is desirable to unveil a suitable way to promote α-Fe_2O_3 in CO_2 photoreduction and related photocatalytic processes.[15]

In the present study, high photothermal reduction of CO_2 with H_2O was achieved with a Fe_2O_3 film using a homemade concentrating solar light reactor system. It was found that Fe_2O_3 film can be partially reduced to form Fe_2O_3/Fe_3O_4 heterojunctions under the high-intensity light irradiation and high-temperature conditions, which greatly promoted the efficiency of CO_2 reduction.

The Fe_2O_3 film was prepared by anodization method. The concentrating light reactor system involving a Fresnel lens was transmission type. Detailed description of the experimental setup can be seen in the Supporting Information (Figures S1 and S2). Figure 1 displays the results of CO_2 photoreduction under given photothermal conditions (Figure 1a shows the result under natural light at room temperature; panels b–d of Figure 1 show the results under high temperature achieved by concentrating solar light). The Fe_2O_3 film exhibits a normal performance at room temperature. CH_4 is detected as the main product, which is consistent with the results of previously reported systems.[16,17] About 3.14 μmol/g_{cata} yield is obtained after 3 h reaction. Under high light intensity and temperature conditions, in addition to CH_4, C_2H_4 and C_2H_6 are also detected as the main gas products. Noticeably, all of the hydrocarbon compounds' yields are boosted from a few μmol/g_{cata} to several hundreds of μmol/g_{cata}. After 3 h reaction, the maximum CH_4 yield can reach 1652.1 μmol/g_{cata}, along with 52.3 μmol/g_{cata} of C_2H_4 and 167.9 μmol/g_{cata} of C_2H_6. The total amount of hydrocarbons based upon single carbon atoms reaches 2092.5 μmol/g_{cata}. The maximum conversion of CO_2 reaches 0.47%. The global conversion is thus about 700 times higher than that obtained under natural light and room temperature. Therefore, the CO_2 photoreduction behavior of Fe_2O_3 film catalyst is significantly improved by highly concentrated sunlight photothermal conditions. Since the increase of the reaction rate was substantial at the light concentrating ratio (CR) of 600, the reasons for the reaction rate boosting under this condition need to be elucidated.

X-ray diffraction (XRD) and SEM analyses were performed for the fresh and used Fe_2O_3 film catalysts, as shown in Figure 2 and Figure S3. The fresh Fe_2O_3 films are mainly amorphous

DOI: 10.1021/acsaem.9b01825
ACS Appl. Energy Mater. 2019, 2, 8376−8380

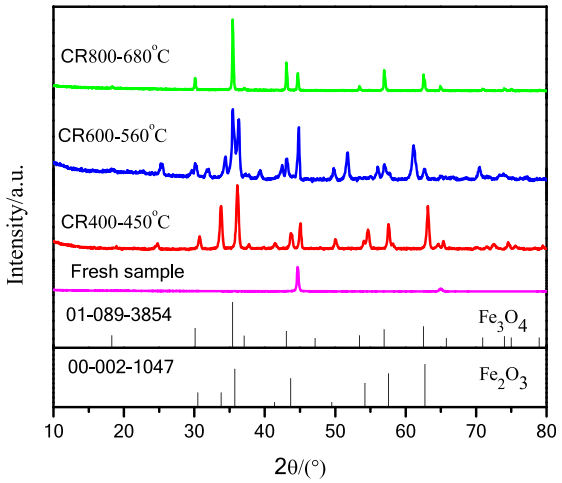

Figure 2. XRD patterns of Fe_2O_3 film before and after reaction under different concentrating ratios (CRs).

with a porous structure. After 2 h reaction, the Fe_3O_4 phase clearly appears on the XRD patterns and coexists with the α-Fe_2O_3 phase, which indicates that Fe_2O_3 was partially reduced to the Fe_3O_4 phase.[18] The more active the catalyst, the clearer the change of the film crystal phase.

X-ray photoelectron spectrometry (XPS) was further performed. XPS spectra were recorded to determine the oxidation states of Fe at the surface of the thin film of α-Fe_2O_3, and the results are shown in Figure 3. In Figure 3A related to the fresh catalyst, three peaks can be observed directly or by deconvolution on the Fe $2p_{3/2}$ curve of fresh α-Fe_2O_3 film at about 710.4, 713.1, and 718.8 eV, respectively. After reaction (Figure 3B), the peak at 718.8 eV was weakened to be nearly vanished, while the other two peaks moved to low binding energy (about 705.8 and 708.8 eV). According to previous reports, the peak position of Fe $2p_{3/2}$ is between 710.6 and 711.2 eV, and the area of the Fe $2p_{3/2}$ peak is greater than that of Fe $2p_{1/2}$. The Fe $2p_{3/2}$ peak has also been associated with a satellite peak located approximately 8 eV higher than the main Fe $2p_{3/2}$ peak for α-Fe_2O_3, and Fe $2p_{3/2}$ of Fe_3O_4 does not have a satellite peak.[19,20] Therefore, the presence of the satellite peak at 718.8 eV in Figure 3A confirms the existence of α-Fe_2O_3; and after reaction, the weakening of the satellite peak implies the reduction of α-Fe_2O_3 Furthermore, the peak position of Fe $2p_{3/2}$ moves downward after reaction, which can be attributed to the formation of Fe^{2+} $2p_{3/2}$ of Fe_3O_4.[21] The XPS spectra thus indicate the reduction of α-Fe_2O_3 to Fe_3O_4 during the reaction.

There is a sharp increase in gas yields between 1.5 and 2 h in Figure 1c. Before 1.5 h, the reaction rate is lower than 400 μmol/(g_{cata}·h), whereas, after 2 h, the reaction rate is clearly higher than 600 μmol/(g_{cata}·•h). Since the reaction conditions do not change, a change in some materials' properties may happen on the α-Fe_2O_3 catalyst during the reaction progress. CO_2 photoreduction was then carried out under the same conditions but stopped at 2 h reaction. The activity and XRD pattern of the used catalyst are presented in Figure S4. The resulting activity is still poor. Only CH_4 and C_2H_4 are detected. The total hydrocarbon yield is below 200 μmol/g_{cata}. Meanwhile, the characteristic peaks of Fe_3O_4 appear, which indicates that α-Fe_2O_3 has been reduced. These results confirm that the formation of Fe_3O_4 is not occurring at the end of the reaction but rather at the initial stage of the reaction. The formation of Fe_3O_4 in the initial stage may act as an activation step for the α-Fe_2O_3 film during CO_2 photoreduction.

Considering that the reaction conditions may be not optimal, further experiment was carried out at concentrating ratio of 600 while reaction temperature was controlled at about 500 °C. The result is shown in Figure S5. In the initial 3 h period, the hydrocarbons' yield increases slowly, and then at 4 h, the yield boosts to reach even higher values. If the initial 3 h is considered as the activation stage, the reaction rates of CH_4, C_2H_4, and C_2H_6 between 3 h and 4 h would reach 1470.7, 736.2, and 277.2 μmol/(g_{cata}·h), respectively. The total hydrocarbons yield rate reaches 3497.5 μmol/(g_{cata}·h), and the CO_2 conversion reaches 0.78%. The solar energy to hydrocarbons efficiency can be calculated to be about 0.05% (Table S1).

From the above results, it can be stated that the activity of CO_2 photoreduction is first improved by the photothermal conditions and then by the change of catalyst properties. The latter reason may be more important. It is known that the CB potential of α-Fe_2O_3 (0.28 eV vs NHE) is more positive than the $CO_2/CO_2^{\bullet-}$ (−1.7 eV), which is unsuitable to reduce CO_2. The CO_2 reduction is often realized by forming heterojunctions or yielding a Z-scheme system with some other semiconductors such as g-C_3N_4. Here, the effect may happen between α-Fe_2O_3 and Fe_3O_4. Although the band gap of Fe_3O_4 in bulk phase can be lower to 0.1 eV, many studies also have shown that the band gap of Fe_3O_4 can reach from 2.2

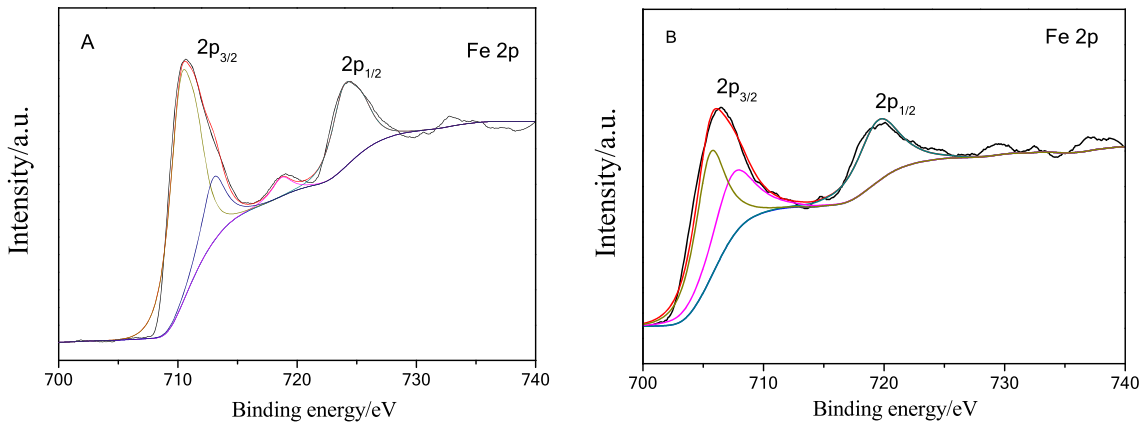

Figure 3. XPS patterns of fresh (A) and used (B) Fe_2O_3 film catalysts.

DOI: 10.1021/acsaem.9b01825
ACS Appl. Energy Mater. 2019, 2, 8376−8380

eV to 3.08 eV in nanoparticles shape. Fe_3O_4 may form a Z-scheme system with Fe_2O_3 which could achieve higher negative potential and realize the CO_2 reduction with H_2O.[15,22−24] The schematic illustration of the reaction mechanism of Fe_2O_3 film is represented in Figure 4.

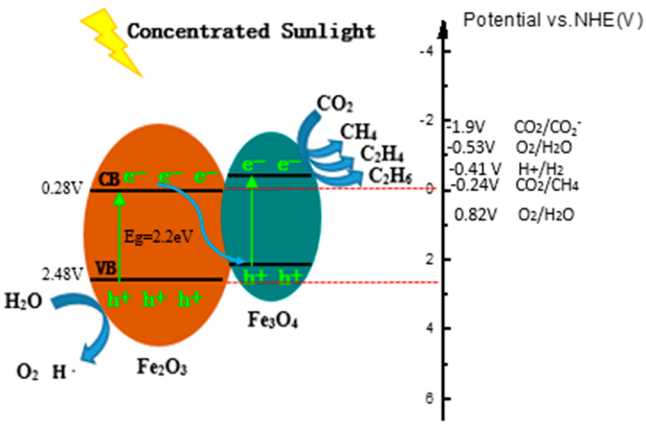

Figure 4. Schematic illustration of reaction mechanism of Fe_2O_3 film.

In summary, we reported for the first time a highly efficient photothermal pathway for CO_2 photoreduction. The study demonstrated that the high photothermal conditions involving concentrated sunlight can effectively activate the Fe_2O_3 film catalyst by forming Fe_2O_3/Fe_3O_4 junctions, thereby enabling one to obtain much higher hydrocarbons yield than the current level, thus outperforming the conventional approach. The catalyst characterization suggests that the formation of the Fe_2O_3/Fe_3O_4 Z-scheme system may account for the high catalyst activity. This method can improve the efficiency of solar energy conversion by utilizing both short and long wavelengths in the solar spectrum, and thus helps with the progress of CO_2 photoreduction.

■ ASSOCIATED CONTENT

Supporting Information

The Supporting Information is available free of charge at https://pubs.acs.org/doi/10.1021/acsaem.9b01825.

Experimental details and additional figures and tables (PDF)

■ AUTHOR INFORMATION

Corresponding Authors

*(Z.Z.) E-mail: zzk@zjut.edu.cn.

*(H.L.) E-mail: luhf@zjut.edu.cn.

ORCID

Zekai Zhang: 0000-0002-4136-5263

Stéphane Abanades: 0000-0002-6689-3652

Notes

The authors declare no competing financial interest.

■ ACKNOWLEDGMENTS

We gratefully acknowledge financial support by the Natural Science Foundation of China (Grant Nos. 21506194 and 21676255).

■ REFERENCES

(1) Shih, C. F.; Zhang, T.; Li, J. H.; Bai, C. L. Powering the future with liquid sunshine. *Joule* **2018**, *2*, 1925−1949.

(2) Gust, D.; Moore, T. A.; Moore, A. L. Solar fuels via artificial photosynthesis. *Acc. Chem. Res.* **2009**, *42*, 1890−1898.

(3) Fujishima, A.; Honda, K. Electrochemical photolysis of water at a semiconductor electrode. *Nature* **1972**, *238*, 37−38.

(4) Chueh, W. C.; Falter, C.; Abbott, M.; Scipio, D.; Furler, P.; Haile, S. M.; Steinfeld, A. High-Flux Solar-Driven Thermochemical Dissociation of CO_2 and H_2O Using Nonstoichiometric Ceria. *Science* **2010**, *330*, 1797−1801.

(5) Weinstein, L. A.; Loomis, J.; Bhatia, B.; Bierman, D. M.; Wang, E. N.; Chen, G. Concentrating Solar Power. *Chem. Rev.* **2015**, *115*, 12797−12838.

(6) Li, X.; Yu, J. G.; Jaroniec, M.; Chen, X. B. Cocatalysts for Selective Photoreduction of CO_2 into Solar Fuels. *Chem. Rev.* **2019**, *119*, 3962−4179.

(7) Roy, S. C.; Varghese, O. K.; Paulose, M.; Grimes, C. A. Toward Solar Fuels: Photocatalytic Conversion of Carbon Dioxide to Hydrocarbons. *ACS Nano* **2010**, *4*, 1259−1278.

(8) Habisreutinger, S. N.; Schmidtmende, L.; Stolarczyk, J. K. Photocatalytic reduction of CO_2 on TiO_2 and other semiconductors. *Angew. Chem., Int. Ed.* **2013**, *52*, 7372−7408.

(9) Choi, K. M.; Kim, D.; Rungtaweevoranit, B.; Trickett, C. A.; Barmanbek, J. T. D.; Alshammari, A. S.; Yang, P. D.; Yaghi, O. M. Plasmon-Enhanced Photocatalytic CO_2 Conversion within Metal−Organic Frameworks under Visible Light. *J. Am. Chem. Soc.* **2017**, *139* (1), 356−362.

(10) Hou, W. B.; Hung, W. H.; Pavaskar, P.; Goeppert, A.; Aykol, M.; Cronin, S. B. Photocatalytic Conversion of CO_2 to Hydrocarbon Fuels via Plasmon-Enhanced Absorption and Metallic Interband Transitions. *ACS Catal.* **2011**, *1*, 929−936.

(11) Sivula, K.; Zboril, R.; Le Formal, F.; Robert, R.; Weidenkaff, A.; Tucek, J.; Frydrych, J.; Grätzel, M. Photoelectrochemical Water Splitting with Mesoporous Hematite Prepared by a Solution-Based Colloidal Approach. *J. Am. Chem. Soc.* **2010**, *132*, 7436−7444.

(12) Shen, S. H.; Lindley, S. A.; Chen, X. Y.; Zhang, J. Z. Hematite heterostructures for photoelectrochemical water splitting: rational materials design and charge carrier dynamics. *Energy Environ. Sci.* **2016**, *9*, 2744−2775.

(13) Stamatiou, A.; Loutzenhiser, P. G.; Steinfeld, A. Solar Syngas Production via H_2O/CO_2-Splitting Thermochemical Cycles with Zn/ZnO and FeO/Fe_3O_4 Redox Reactions. *Chem. Mater.* **2010**, *22*, 851−859.

(14) Bush, H. E.; Loutzenhiser, P. G. Solar electricity via an Air Brayton cycle with an integrated two-step thermochemical cycle for heat storage based on Fe_2O_3/Fe_3O_4 redox reactions: Thermodynamic and kinetic analyses. *Sol. Energy* **2018**, *174*, 617−627.

(15) Jiang, Z. F.; Wan, W. M.; Li, H. M.; Yuan, S. Q.; Zhao, H. J.; Wong, P. K. A Hierarchical Z-Scheme α-Fe_2O_3/g-C_3N_4 Hybrid for Enhanced Photocatalytic CO_2 Reduction. *Adv. Mater.* **2018**, *30*, 1706108.

(16) Wang, J. C.; Zhang, L.; Fang, W. X.; Ren, J.; Li, Y. Y.; Yao, H. C.; Wang, J. S.; Li, Z. J. Enhanced photoreduction CO_2 activity over direct Z-scheme α-Fe_2O_3/Cu_2O heterostructures under visible light irradiation. *ACS Appl. Mater. Interfaces* **2015**, *7*, 8631−8639.

(17) Hsu, Y. K.; Chen, Y. C.; Lin, Y. G. Novel ZnO/Fe_2O_3 Core-Shell Nanowires for Photoelectrochemical Water Splitting. *ACS Appl. Mater. Interfaces* **2015**, *7*, 14157−14162.

(18) Mohapatra, S. K.; John, S. E.; Banerjee, S.; Misra, M. Water Photooxidation by Smooth and Ultrathin α-Fe_2O_3 Nanotube Arrays. *Chem. Mater.* **2009**, *21*, 3048−3055.

(19) Tahir, A. A.; Wijayantha, K. G. U.; Saremi-Yarahmadi, S.; Mazhar, M.; McKee, V. Nanostructured Fe_2O_3 Thin Films for Photoelectrochemical Hydrogen Generation. *Chem. Mater.* **2009**, *21*, 3763−3772.

(20) Li, L. L.; Chu, Y.; Liu, Y.; Dong, L. H. Template-Free Synthesis and Photocatalytic Properties of Novel Fe_2O_3 Hollow Spheres. *J. Phys. Chem. C* **2007**, *111*, 2123−2127.

DOI: 10.1021/acsaem.9b01825
ACS Appl. Energy Mater. 2019, 2, 8376−8380

(21) Leduc, J.; Goenuellue, Y.; Ghamgosar, P.; You, S.; Mouzon, J.; Choi, H.; Vomiero, A.; Grosch, M.; Mathur, S. Electronically-Coupled Phase Boundaries in α-Fe_2O_3/Fe_3O_4 Nanocomposite Photoanodes for Enhanced Water Oxidation. *ACS Appl. Nano Mater.* **2019**, *2*, 334−342.
(22) Kouotou, P. M.; Kasmi, A. E.; Wu, L. N.; Waqas, M.; Tian, Z. Y. Particle size-band gap energy-catalytic properties relationship of PSE-CVD-derived Fe_3O_4 thin films. *J. Taiwan Inst. Chem. Eng.* **2018**, *93*, 427−435.
(23) Xu, Y.; Schoonen, M. A. A. The absolute energy positions of conduction and valence bands of selected semiconducting minerals. *Am. Mineral.* **2000**, *85*, 543−556.
(24) Zhao, Y.; Sadat, M. E.; Dunn, A.; Xu, H.; Chen, C. H.; Nakasuga, W.; Ewing, R. C.; Shi, D. L. Photothermal effect on Fe_3O_4 nanoparticles irradiated by white-light for energy-efficient window applications. *Sol. Energy Mater. Sol. Cells* **2017**, *161*, 247−254.

DOI: 10.1021/acsaem.9b01825
ACS Appl. Energy Mater. 2019, 2, 8376−8380